



Provided by the author(s) and NUI Galway in accordance with publisher policies. Please cite the published version when available.

Title	A comparative study of the effect of varied reaction environments on a swirl stabilized flame geometry via optical measurements
Author(s)	Banyon, Colin; Rodriguez-Henriquez, Jose J.; Paterakis, George; Malliotakis, Zisis; Souflas, Konstantinos; Keramiotis, Christos; Vourliotakis, George; Mauss, Fabian; Curran, Henry J.; Skevis, George; Koutmos, Panagiotis; Founti, Maria
Publication Date	2018-01-04
Publication Information	Banyon, Colin, Rodriguez-Henriquez, Jose J., Paterakis, George, Malliotakis, Zisis, Souflas, Konstantinos, Keramiotis, Christos, Vourliotakis, George, Mauss, Fabian, Curran, Henry J., Skevis, George, Koutmos, Panagiotis, Founti, Maria. (2018). A comparative study of the effect of varied reaction environments on a swirl stabilized flame geometry via optical measurements. <i>Fuel</i> , 216, 826-834. doi: 10.1016/j.fuel.2017.09.105
Publisher	Elsevier
Link to publisher's version	https://doi.org/10.1016/j.fuel.2017.09.105
Item record	http://hdl.handle.net/10379/14789
DOI	http://dx.doi.org/10.1016/j.fuel.2017.09.105

Downloaded 2020-10-17T04:51:25Z

Some rights reserved. For more information, please see the item record link above.



Chapter 10

A comparative study of the effect of varied reaction environments on a swirl stabilized flame geometry via optical measurements

Published in *Fuel* Volume 183, pages 372–385 in 2017.

DOI: <https://doi.org/10.1016/j.combustflame.2017.05.017>

Authors and Contributions

- (1) **Colin Banyon**
National University of Ireland, Galway
Contribution: Experimental measurements, data analysis, and manuscript preparation.
- (2) **Jose J. Rodriguez-Henriquez**
Brandenburg University of Technology
Contribution: Experimental measurements and manuscript preparation.
- (3) **George Paterakis**
University of Patras
Contribution: Experimental measurements and data analysis.
- (4) **Zisis Malliotakis**
National Technical University of Athens
Contribution: Experimental measurements and manuscript preparation.
- (5) **Konstantinos Souflas**
University of Patras
Contribution: Experimental measurements.

- (6) **Christos Keramiotis**
National Technical University of Athens
Contribution: Project Management, experimental measurements, and manuscript review.
- (7) **George Vourliotakis**
National Technical University of Athens
Contribution: Project Management and manuscript review.
- (8) **Fabian Mauss**
Brandenburg University of Technology
Contribution: Project Management and manuscript review.
- (9) **Henry J. Curran**
National University of Ireland, Galway
Contribution: Project management and manuscript review.
- (10) **George Skevis**
Centre for Research and Technology Hellas (Greece)
Contribution: Project management and manuscript review.
- (11) **Panagiotis Koutmos**
University of Patras
Contribution: Project management and manuscript review.
- (12) **Maria Founti**
National Technical University of Athens
Contribution: Project management and manuscript review.

Abstract

The present work is a part of a larger experimental campaign which examines the behaviour of various fuels on a swirl stabilized flame burner configuration. Overall, detailed speciation measurements and temperature measurements were combined with optical measurements. The work presented here concerns the part of the experimental campaign which deals with the optical characteristics of the examined flames. The work adds to the growing database of experimental measurements assessing engine-relevant reaction environments which shift from traditional ones in order to meet pollutant emission regulations and efficiency standards. Here, the oxidation of several commonly used fuel and fuel surrogates that are subjected to the addition of a bio-derived fuel additive (dimethyl ether) and emulated exhaust gas recirculation (EGR) is studied in a laboratory-scale swirl stabilized burner. The natural flame chemiluminescence has been exploited to selectively measure line of sight CH* and OH* profiles for combinations of these fuels and reaction environments. As a result, the geometry and intensity of the reaction and oxidation zones have been parametrically evaluated for

a sizable number of initial conditions. From an analysis of the collected data, a chemical uniqueness in methane and propane flames has been found along with a change in flame topology as a function reactant temperature and dilution with inert gases, while the flames were virtually unaffected by all other variations in reaction conditions. This insensitivity provides confidence in the use of tailored in-cylinder fluid dynamic/chemical interactions to extend engine operating conditions to otherwise difficult regimes.

10.1 Introduction

The Paris Agreement has set ambitious targets for the worldwide reduction of toxic and greenhouse chemical emissions into the atmosphere [1]. Consecutively, engine manufacturers are facing legislative constrains which are expected to tighten the already stringent pollutant limits for future engines. In recent years, these perpetually expanding regulations, along with concerns over fossil fuels scarcity, have led to a large aggregate of research concerning the extrapolation of conventional combustion strategies that have been used in engines and combustors to more clean, efficient, and fuel flexible regimes [2]. This research has led to several techniques which have been largely adapted nowadays by commercially available internal combustion engines (ICEs), such as, exhaust gas recirculation [3], down-size and boost [2], and bio-derived fuel additives [4]. Other, more long-term solutions have also been suggested, which promise even more significant improvements in engine efficiency and fuel flexibility and emission performance [5]. These advanced engine regimes [6–8] typically employ a more chemical kinetically controlled combustion strategy at lower temperature and leaner conditions than conventional ICEs. Unfortunately, combustion control throughout the engine operating map and low reaction propagation stabilities at these fuel lean operating regimes may occur [5]. Efforts to reassure the effectiveness of the aforementioned techniques as well as to mitigate challenges with longer term solutions has spawned a plethora of research trying to understanding the tightly coupled fluid dynamic and fuel chemistry interactions [8–9]. Several studies have focused on studying these interactions directly in engines [10,11], but conventional diagnostics used in apparatuses with no optical or physical in-situ in cylinder access have been proved challenging [12,13], and although in some cases, the arduous task of mounting ample diagnostics to laboratory engine rigs has proved successful [14], the ability to extrapolate these results to other combustion platforms is a straight forward process. On the other hand, the use of comprehensive laser-based diagnostics does not unravel entirely all difficulties since the compromise for achieving the optical access is the difficulty to achieve otherwise trivial in-cylinder conditions to such as compression ratios and the accompanied heat losses [15]. As a result, researchers try to combine a variety of analytical and optical methodologies in similar or based on previous results on similar test rigs to acquire the maximum synergy and describe to the best possible degree a given engine behavior [16]. To generalize experimental findings, fuel oxidation experiments can be conducted in well-characterized, laboratory-scale reactors as a function of physical state parameters [17,18]. Typically, data regarding the reacting flow is then utilized as validation targets for fundamental fluid dynamic and chemical models, which collectively act as simulation tools for the

more complex cases. Unfortunately, these transport models for typical in-cylinder environments quickly become heavily restrained by the available computational capabilities. While a large body of work has focused on measurements tied to specific combustors as well as the development of fundamental physics models, there is a limited amount of informatic data [e.g. 19, 20] for the generic reactive in-cylinder flow environments. On the other hand, swirl burners have been commonly used in a variety of combustion applications, ranging from utility boilers and gas turbines to coal combustors. These also represent convenient laboratory scale test beds, for the direct application of a range of experimental techniques in the study of the combined effects of flame stabilization, mixture dilution, inlet conditions and emission performance for the development of a wide variety of technical combustion systems [21–23]. More specifically, in recent experimental work [24], stereoscopic particle induced velocimetry (SPIV), together with planar induced fluorescence of OH radicals, and chemiluminescence have been used in order to depict flow fields and to capture reaction zones and flame stabilization regions. The effect of dilution with CO₂ and H₂O in methane and DME flames on NO formation has, also, been examined along with mathematical modeling [25], and correlations of the chemical effect of dilution on emissions have been discussed on the basis of the local chemistry and its interaction with the inlet conditions. The effects of CO₂ addition have been studied in [26] through chemical analysis of the participating radicals and reactions, over a range of flame conditions.

This study presents the first in a campaign by the current author list to examine the behaviour of various fuels on the given setup under conditions frequently met in practical applications. Overall, detailed speciation measurements and temperature measurements were combined with optical measurements and the work presented here concerns the part of the experimental campaign which deals with the optical characteristics of the examined flames. The study on the one hand adds to the database of immediately useful fuel oxidation data for a generic commercial combustor and on the other hand serves as a means of evaluating operating parameters such as dilution, preheating and fuel interchange in engine related conditions. More specifically, the study is facilitated by flame chemistry measurements of a wide variety of fuels that are used as fuels or fuel surrogates in automotive, marine and aviation transportation engines along with bio-derived fuel dopants and added diluent gases that represent the exhaust gas recirculation cycles of an operating engine. Furthermore, the burner has been configured to generate a swirling flow at the nozzle exit to emulate a swirl flame-stabilization technique that has been proposed for engines running in a lean operation mode [27]. While the current laboratory burner does not exactly reproduce the reactive in-cylinder environment of an ICE, it offers effortless optical access and control, and therefore a straightforward coupling of standard analytical chemistry instruments to the rig in order to probe the chemical characteristics of the reacting flow. Nonetheless, there are significant differences in flame formation, confinement, hence pressure conditions which need to be seriously taken into account when comparing the findings of the present work with engine studies. In the current study, the line of sight natural luminosity of the flame has been measured simultaneously for selective OH* and CH* chemiluminescence emission bands, which can be considered good markers to monitor heat release oscillations and heat

release rates as mentioned in [28–29]. However, effects of the turbulence intensity, strain rate, flame front curvature, mixture composition, temperature and pressure and fuel type need to be included to obtain quantitative heat release rate correlations [28–35]. The obtained images are then deconvolved into constructs that define the geometry of the reactive and oxidative flame zones, where changes to the flame structure are then correlated to changes in the operating conditions. These data may potentially be used to understand the effect that unconventional utilized fuel blends and varying operation parameters could have on flame characteristics.

10.2 Experimental methodology

10.2.1 Swirl burner configuration

The NTUA swirl burner platform has been previously described [36], however a more contemporary description of the current arrangement of the rig is provided here. A schematic of the burner fluid handling and control system is shown in Fig. 10.1, and should be referenced in regard to the discussion presented in this sub-section. The burner exit jet (21 mm inner diameter and 27 mm outer diameter) receives a steady flow of fuel and air in a separated coaxial arrangement, which is allowed to mix 12 mm upstream of the burner exit nozzle [37]. The burner used in this study differs from conventional research burners that are used to isolate chemical kinetic processes in flames (for example [38–40]) in that a specially designed air stream geometry is used directly upstream of the burner exit nozzle that creates a swirling flow downstream of the burner exit nozzle. This swirling flow acts as a reaction zone containment mechanism for the flame and provides flame stabilization at chemically unreactive conditions, and has been used as a technique in commercial burners [41] and engines [42] to extend operating conditions to low pollutant forming regimes. The NTUA swirl burner splits the air stream into three geometrically fixed sub-streams directly upstream of the exit nozzle and redirects a portion of the flow into two opposed ports that are tangent to the circumference of the exit nozzle, which provides angular flow momentum that subsequently creates a swirling motion at the burner surface. In the current burner setup, the air stream is composed of air along with any gaseous or vaporized diluents of interest. For the current study, dried shop air is regulated into the burner air stream using a Bronkhorst (model number F-203AV-1M0) mass flow controller (MFC). Any additional gaseous diluents (N_2 and CO_2) are supplied and mixed into the air stream within a manifold far upstream of the burner from research grade pressurized cylinders, where supply volumetric flow rates are also controlled using Bronkhorst MFCs. The air stream passes through, and may be heated by, an electric honeycomb heater that is situated between the MFCs and burner exit nozzle. The energy supplied to the pre-heating unit is controlled via a proportional-integral-derivative (PID) feedback loop, where the feedback signal from an S-type thermocouple that is mounted in the burner exit nozzle is compared to a desired surface temperature. For heated experiments, water may also be added to the air stream. This is achieved in the current setup by supplying liquid water from a peristaltic pump to

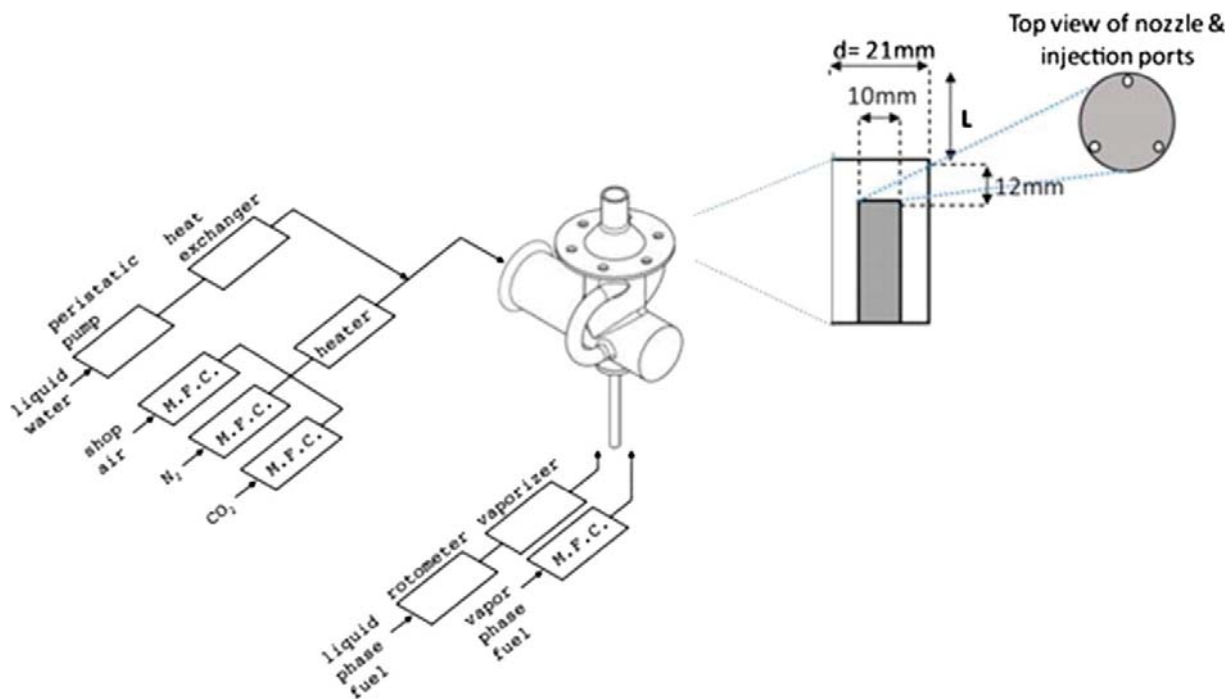


Figure 10.1: An illustration of the air, fuel and diluent plumbing and control system of the NTUA swirl burner.

an inner, coaxial heat exchanger/vaporizer tube within, and exiting into, the hot air stream carrier pipework. The mass flow rate of water into the air stream is adjusted by varying the voltage supplied to the peristaltic pump, where voltage to average-mass-flow calibration curves are generated for the device by offline liquid mass collection measurements over 5 min. Both liquid and vapor phase fuels can be supplied to the burner by utilizing two independent feed systems. Vapor phase fuels are directly supplied to the fuel supply from pressurized cylinders, where the volumetric flow rate of these flows is regulated using a Bronkhorst MFC (model F-202AV-M201). However, the flow rate of dimethyl ether (DME) in particular is regulated into the flame using a rotometer with the calibration criteria suggest by Ref. [43] due to the corrosive nature of the fuel which causes damage to MFC components. Liquid phase fuels may be supplied through a pneumatically driven pump, where the liquid fuel supply mass flow rate is throttled using a needle valve. In this method, the mass flow rate of liquid is correlated to needle valve choke in an offline calibration, where the average mass flow of the fuel over 5 min. is determined by collecting and weighing the mass from the feed device. Downstream of the flow control needle valve, the fuel is vaporized in an electrically heated, stainless steel tube before arriving at the burner surface. The heater surrounding the vaporizer tube is supplied with a variable voltage in order to transfer a sufficient power to the liquid fuel to fully vaporize the liquid, which is verified offline.

10.2.2 Flame chemiluminescence measurements

The fuel oxidation process in flames provides sufficient energy to the reacting gas to cause a transition in the molecular vibrational modes and some low-lying electronic configurations for combustion intermediates that subsequently lead to a collective broadband photon emission of the excited state species as it quenches to ground state. This natural, chemical reaction induced chemiluminescence in flames can be taken advantage of as a means to probe the physical/chemical properties of the reacting gases, which is the case in this study. More specifically, this study is interested in tracking changes to the oxidation and heat release front geometries in swirl flames, when exposed to reaction environments that modern engines experience to achieve compliancy with pollutant formation and efficiency regulations. In the present study, simultaneous images of both OH* and CH* were collected by employing a double image (I) projection optical system for the spectral separation of flame emitted light (A), developed and constructed in the Laboratory of Applied Thermodynamics. The optical configuration consists of two spectral filters, a system of mirrors and an optical lens (Fig. 10.2). First, light from the flame was transmitted through two, narrow band-pass LaVision filters centered at 307 nm (B1) and 433 nm (B2) respectively, both with a full width at half maximum of 10 nm, onto a system of mirrors. Subsequently, a fully reflective first surface mirror (reflectance of 85%) (C) was employed to reflect the incoming light onto a second fully reflective first surface mirror (D), which redirects the light into the IRO unit (G) and the CCD (H) camera via an achromatic triplet lens (f/4, 193–1000 nm) (E). The spatial distribution of the emitting species was recorded by the CCD camera for the variety of studied conditions (i.e. introduction of DME, EGR, different levels of preheating etc.). Image processing was performed using the Davis 8.0 software (LaVision). Averages were extracted from five hundred instantaneous images, which were recorded at a frequency of 14 Hz. The signal to noise ratio was greater than 8:1 and the exposure time was 2.1 ms. The highest CCD resolution was at 1626 x 1236 pixels and the spatial resolution of the captured images was at 9.75 x 8.25 pixels/mm. As the experimental measurements were effectively a 2D image of projected line of sight measurements from a cylindrically symmetric process, an Abel transform, as suggested in [44], was applied to extract two-dimensional information from these images [45,46]. Chemiluminescence is very helpful in providing some of the characteristics of the flame topology. The monitored species are considered useful indicators of flame behaviour i.e. OH* defines the oxidation zone, while CH* defines the flame front and the heat release zone. Similar methodologies have been applied in the past [47]. Nonetheless, the overall chemiluminescence spectrum at a specified location of the flame was not available at the course of this work, as a high sensitivity light spectrometer [48] was required. For the same reason, no information for the quantification of CO₂* emission could be extracted. Nevertheless, for electronically excited carbon dioxide it is known that it is proportional to the product of concentrations of CO and O, as well as its chemical kinetics are not completely defined [49].

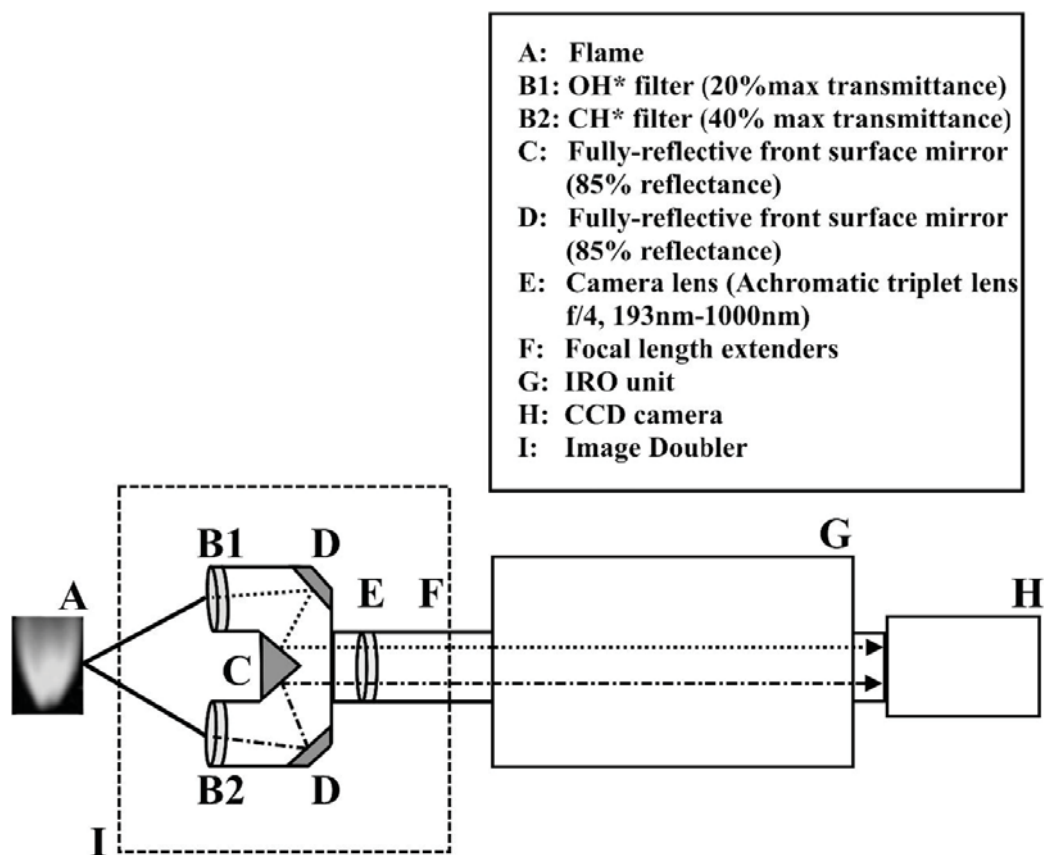


Figure 10.2: An illustration of the technique used to selectively measure the chemically induced chemiluminescence of the flame.

10.2.3 Experimental matrix

This study investigates the chemiluminescence of swirl flames produced with a number of vapor and liquid phase transportation relevant fuels; methane, propane, hexane, heptane, 2,2,4-trimethylpentane (*iso*-octane), and decane. Here, methane and propane are used as chemical surrogates for natural gas, liquified natural gas and liquified petroleum gas. The primary reference fuels heptane and *iso*-octane are used here to represent diesel and gasoline fuels, respectively. Further, hexane is used as jet fuel representative, while decane is used as a generic proxy of heavier components in liquid transportation fuels.

Spectrally filtered images are collected for flames of each neat fuel as well as for flames where 10% of the neat fuel stream mass is replaced by DME, in an attempt to investigate the effect of doping fossil fuels with bio-derived additives. In this vein, the effect of DME addition to methane and propane flames was further investigated by replacing the neat fuel with 20, 30, and 50% DME.

For all of the cases presented here, the mass flow rate of fuel to each flame has been constrained to result in a 5 kW steady state heat release ($\dot{m}_f = \text{HHV}/5 \text{ kW}$). Detailed information about the flow rates used can be obtained from Table ???. Once the mass

Table 10.1: The detailed composition of the reactant mixtures in jet-stirred reactor experiments.

Fuel	10% DME add.	10% Dil. add.	Fuel Flow [L/min]	Air Flow [L/min]	Dil. Flow [L/min]	Tot. Flow [L/min]	Dev. [%]
methane			8.36	80.5	0.00	88.86	3
		×	8.36	80.5	9.88	98.74	14
	×		7.83	79.3	0.00	87.13	1
	×	×	7.83	79.3	9.68	96.81	12
propane			3.22	79.0	0.00	82.22	-5
		×	79.0	80.5	9.14	91.36	5
	×		3.33	78.6	0.00	81.93	-5
	×	×	3.33	78.6	9.10	91.03	5
<i>n</i> -heptane			0.0095	78.9	0.00	78.91	-9
		×	0.0095	78.9	8.77	87.68	1
	×		0.1749	78.7	0.00	78.87	-9
	×	×	0.1749	78.7	8.76	91.03	1
<i>n</i> -decane			0.0093	79.5	0.00	79.51	-8
		×	0.0093	79.5	8.83	88.34	1
	×		0.1287	79.4	0.00	79.53	-8
	×	×	0.1287	79.4	8.84	88.37	2

flow rate of fuel has been determined, the mass flow rate of air to the burner was varied to produce a globally stoichiometric fuel-to-oxidizer ratio, and additionally methane flames were also generated at a globally lean condition ($\phi = 0.5$) to investigate the effects of lean operation.

The influence of initial reactant temperature on flame structure has been isolated in this study by varying the level of preheating of the air stream to arrive at two burner surface temperatures for each case. For initially vapor phase fuels (methane and propane), flames with the burner surface at room temperature (approximately 25 C) and 300 C were carried out. Unfortunately, experiments with the initially liquid fuels (hexane, heptane, *iso*-octane, and decane) could not be performed at room temperature (nor at a pre-heat temperature of 105 C in the case of decane) due to the tendency of these vaporized fuels to condense when mixed with the cooler air stream before arriving at the reaction front. Therefore, for these fuels a burner surface temperature of 105 C and 300 C was selected in order to avoid over saturation of the vaporized fuels upstream of the flame.

The effect of mixture dilution on each fuel was assessed by adding N₂, CO₂, and H₂O to the air stream. More specifically, two diluent compositions were chosen, which are referred to in the remainder of this manuscript as “dry dilution” and “wet dilution”. The composition of these mixtures has been chosen in order to resemble the composition of an typical EGR utilized in engines [29]. Dry dilution refers to a 90/10 mixture of N₂/CO₂ (by volume) which is added to the air stream at a volumetric flow rate that is 10% of the combined fuel and air flow rate ($\dot{V}_d = 0.1(\dot{V}_f + \dot{V}_a)$). Cases with wet dilution contain the dry dilution diluent feed into the air stream as well as the addition of vaporized water into the air stream at a liquid

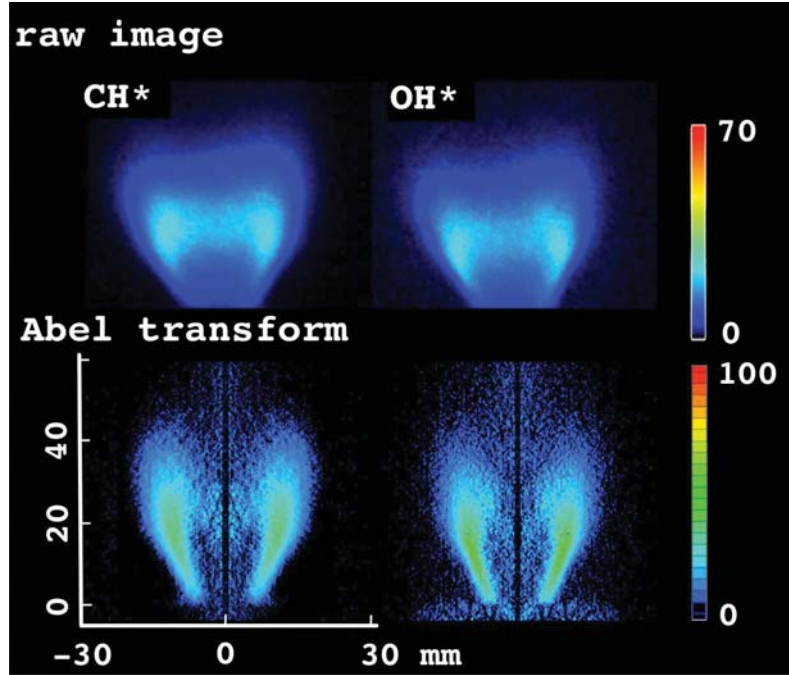


Figure 10.3: An example raw spectrally filtered image for CH* and OH* profiles, along with the Abel transform of the raw image. Arbitrary units. The example case is a neat *iso*-octane flame with a burner surface temperature of 105 C.

volumetric flow rate that is 0.05% of the combined fuel and air flow rate ($\dot{V}_{w,i} = 0.05(\dot{V}_f + \dot{V}_a)$). Dilution was investigated for each neat and doped fuel, where dry dilution was applied at the lower pre-heating echelon and wet dilution to the higher level of pre-heating due to the inadequate vaporization of water in the air stream at lower temperatures.

10.3 Experimental Results

Both the CH* and OH* profiles for a total of 59 swirl flames were imaged following the experimental methodology and matrix detailed above. For all of these conditions, a steady-state conical flame was stabilised at the edge of the bluff body face through recirculation of the combustion products onto the incoming fresh mixture layer. The process was assisted by the induced swirl motion.

For the sake of brevity the raw images of these flames are not presented in this text, however an example image is shown in Fig. 10.3 while the complete data set is available in the Supplemental Material. The subsequent methods to post-process and decompose the raw flame images into comparable metrics in order to achieve an adequate comparison of flame luminosities and geometries throughout the wide range of conditions that were considered is presented in the remainder of this section.

The raw flame images suffer from an integrated mapping of photon emission profiles

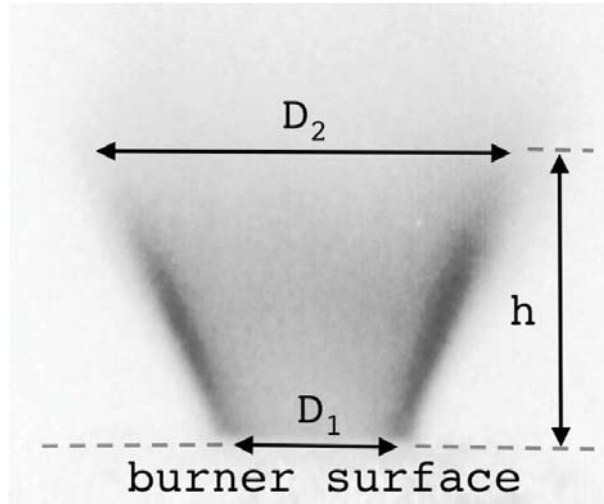


Figure 10.4: The definition of spatial flame parameters used to compare flame geometries.

around the entire three-dimensional flame projected onto the two-dimensional CCD surface, which is demonstrated in Fig. 10.3. An Abel transform of the example case is also presented in Fig. 10.3, where a more well-defined reaction front can be observed compared to the raw image. All flame images in this study have undergone Abel transformations, and all of the results in this study (in regard to both flame luminosity and geometry) have been drawn from these processed images. It should be noted here, that a slight asymmetry about the burner exit nozzle axis was observed in many of the flames, which marginally compromises the validity of transformed results. The asymmetry was systematic for all flames investigated and was only minor compared to the magnitude of the parameters assessed i.e. D_1 , D_2 , and H . This asymmetry is a result of mixing but could not be correlated with any of the changes in conditions.

Experimental information regarding the geometry of each flame has been further compressed in terms of the three conical parameters defined in Fig. 10.4, which fully defines the simplified geometry of the flame. These three parameters, however, offer themselves as simple and easily traceable metrics that can be readily used to compare the large data set at hand. The diameters, D_1 and D_2 , are measured from flame images as double the horizontal distance between the burner exit nozzle centerline and the outer edge of the reaction front. The outer edge is detected as the last observable pixel while horizontally moving away from the burner centerline, where observable pixels are considered to have a higher intensity value than the background noise. The diameters D_1 and D_2 are further constrained vertically as crossing through the first and last observable pixel along the entire horizontal axis while moving vertically from the burner surface in the bulk flow direction. The flame height, H , is taken to be the vertical distance between D_1 and D_2 . These simplified metrics, as standalone measurements, offer little potential use beyond the scope of this study, and should be treated as rough metrics to assess comparative trends between the flames presented here.

Much in the same vein as the above discussion of geometrical parameters, simplified

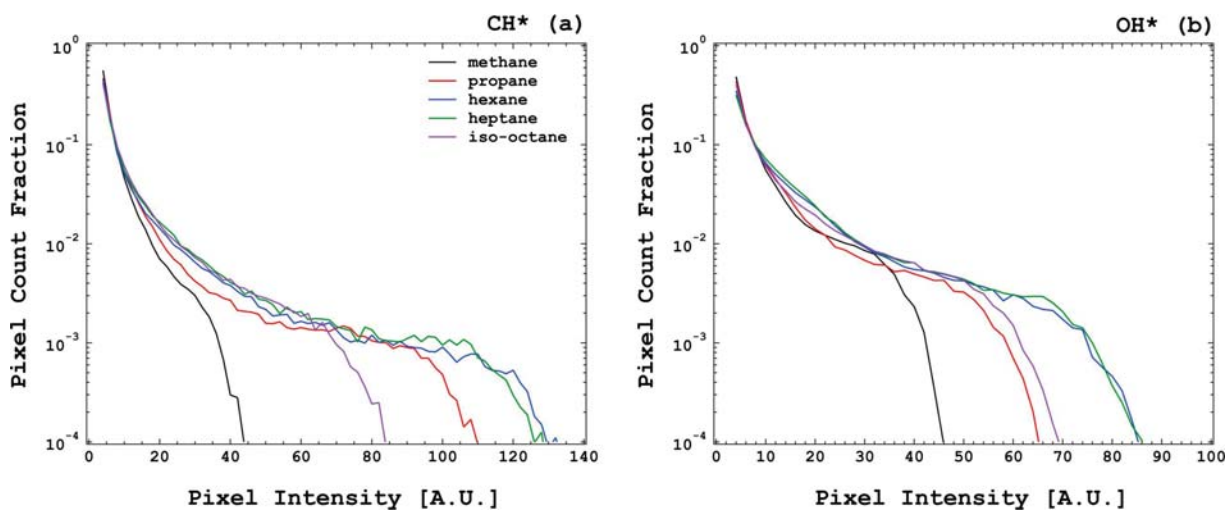


Figure 10.5: The definition of spatial flame parameters used to compare flame geometries.

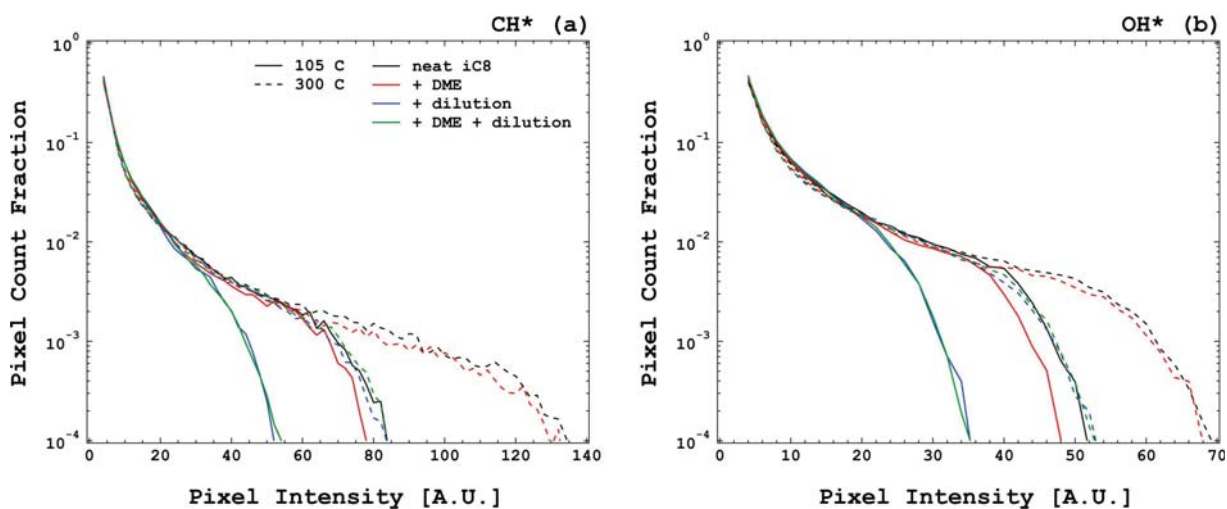


Figure 10.6: (a) CH^* and (b) OH^* luminescence intensity statistics for varied neat *iso*-octane reaction environments.

metrics for flame intensities have been extracted from the large, line of sight images in order to compare the relative amount of CH^* and OH^* produced within each flame, across the range of considered conditions. However, choosing appropriate simplified metrics for flame intensities was not as trivial of a process as the selection of geometrical parameters. In order to choose appropriate intensity metrics, a statistical analysis was performed on the line of sight images for a small subset of the investigated flames. This analysis is summarized in Figs. 10.5 and 10.6, which show the fraction of pixels within an image which have a given intensity, without considering spatial position, for stoichiometric flames of varied neat fuels as well as for *iso*-octane flames under all varying initial conditions, respectively. The pixel fraction disregards any pixels with an intensity lower than the background intensity along

with any reflections from the burner surface. A typical distribution of pixel intensities for CH^* and OH^* quickly becomes apparent from the inspection of these figures, where the pixel fraction at a given intensity rapidly decays at similar rates with increasing intensity for each flame until each case exits this clustered curve at the maximum intensity. Due to the nature of this correlative behavior between investigated flames, we recognize both the maximum pixel intensity and area integrated pixel intensity as sufficient metrics to compare image intensity distributions between the investigated cases in the current study.

10.4 Discussion

A comparison of flame CH^* and OH^* intensities and geometries is presented here, in terms of the metrics described above, which is shown in Figs. 10.7, 10.8 and 10.9. Figure 7 depicts the integrated and maximum CH^* and OH^* signals in each flame image, where the data for each fuel and burner surface temperature are lumped together for each simulated engine operating condition. On the other hand, the geometrical parameters that were derived from the CH^* and OH^* profiles for each flame are illustrated in Figs. 10.8 and 10.9, respectively, where data sets have been grouped in a manner that is consistent with the measured intensity parameters. A pronounced trend appears in Fig. 10.7 across all of the varied reaction environments for both the CH^* and OH^* emission intensities, where these intensities increase with molecular size for methane through hexane then remains constant with any further increase in molecular size. Moreover, only a small change in feed volumetric flow rates ($\pm 10\%$) was necessary to achieve a constant flame power and stoichiometry, where changes in the flame fluid dynamics should be considered small enough allowing for a direct comparison of all flames.

Due to these consistencies when comparing flames of different fuels, a degree of uniqueness in flame chemical kinetics is hypothesized to exist for methane and propane, while a loss of chemical individuality is thought to occur for the larger molecular structures. The data presented in Figs. 10.8 and 10.9 suggest that this difference in chemical kinetics between swirl flames of varied fuels is not directly contained in the preferred oxidation pathways due to a nearly constant geometry throughout comparisons of these test cases, albeit within the error of the simplified metrics that were used. Rather, a difference in the chemical kinetic pathways leading to the production of the excited CH^* and OH^* molecules in methane and propane swirl flames compared to the other fuels tested is suspected to be responsible for the lower intensity signals for these fuels. For instance, CH^* is mainly produced from the oxidation of intermediate acetylene produced during the combustion process [50]. For methane in particular, acetylene is mainly produced from the decomposition of ethane, which is in turn produced from the unfavored recombination of methyl radicals. On the other hand, larger molecules have a more direct decomposition route to acetylene. In short, it is difficult to discern whether a bulk effect is induced on swirl flames using smaller alkanes than larger ones, due to potentially artificial changes in chemiluminescence signals caused by differing preferential pathways between fuels to the chemical markers used in this study. Unfortunately, the current data set is unequipped to qualify this hypothesis, and an opportunity for

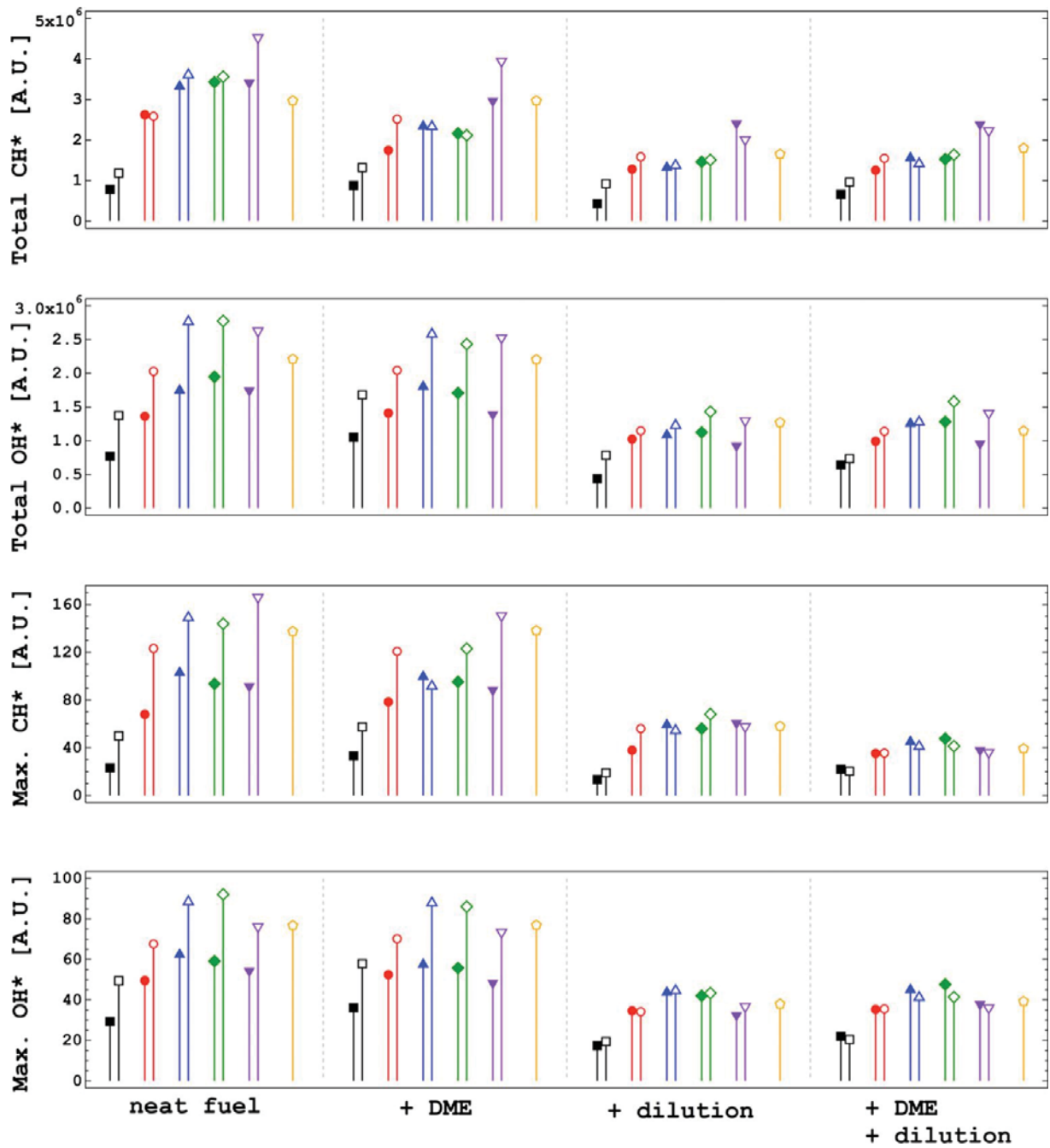


Figure 10.7: Measured maximum and integrated CH* and OH* chemiluminescence intensities for swirl flames subjected to various reaction environments. Closed symbols correspond to lower initial reactant temperatures, while open symbols correspond to higher initial reactant temperatures. Black squares, methane; red circles, propane; blue upward pointing triangles, hexane; green diamonds, heptane; purple downward pointing triangles, *iso*-octane; orange pentagons, decane.

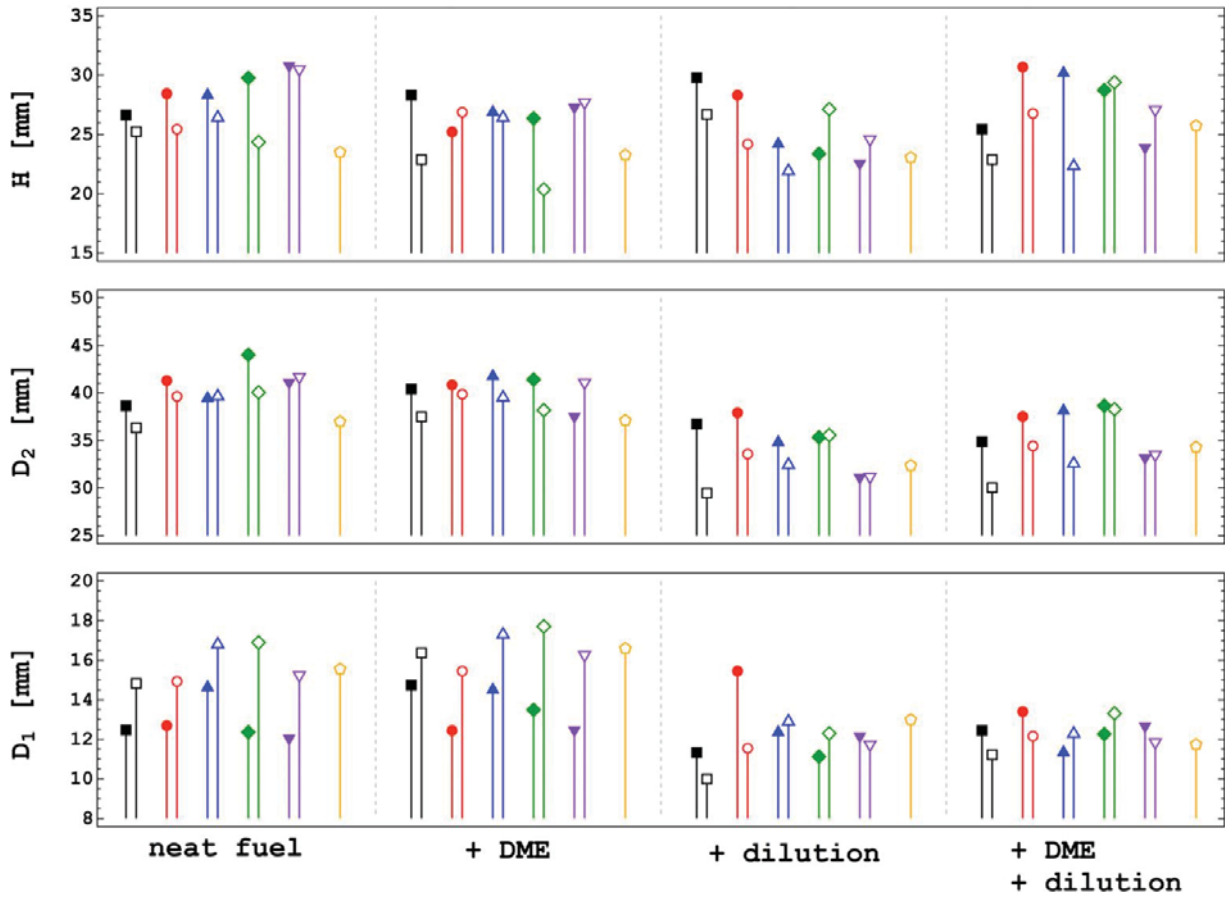


Figure 10.8: Measured conical geometric parameters of swirl flame CH^* profiles subjected to various reaction environments. Closed symbols correspond to lower initial reactant temperatures, while open symbols correspond to higher initial reactant temperatures. Black squares, methane; red circles, propane; blue upward pointing triangles, hexane; green diamonds, heptane; purple downward pointing triangles, *iso*-octane; orange pentagons, decane.

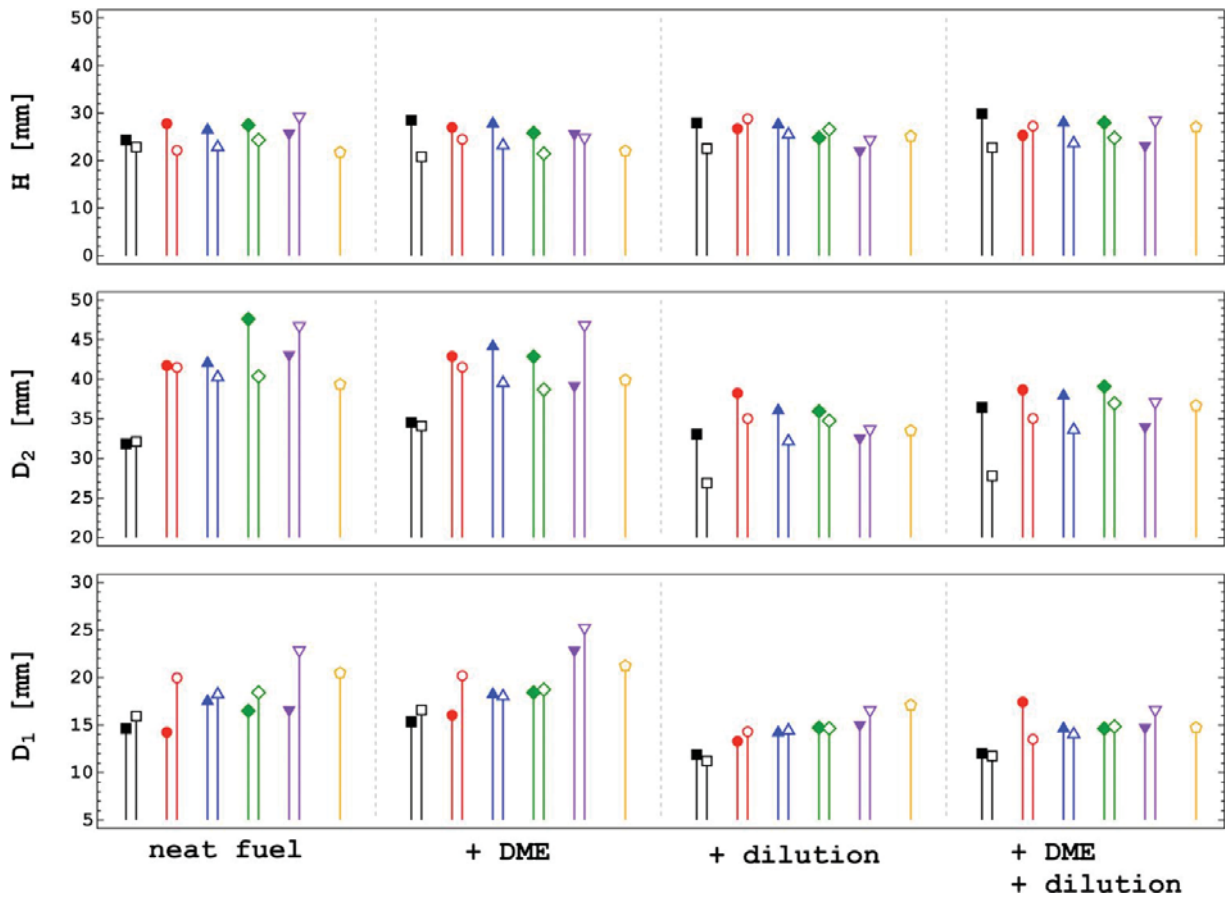


Figure 10.9: Measured conical geometric parameters of swirl flame OH* profiles subjected to various reaction environments. Closed symbols correspond to lower initial reactant temperatures, while open symbols correspond to higher initial reactant temperatures. Black squares, methane; red circles, propane; blue upward pointing triangles, hexane; green diamonds, heptane; purple downward pointing triangles, *iso*-octane; orange pentagons, decane.

future work is noted.

A clear trend is also observed in both flame intensity and geometry as function of initial reactant temperatures. In most cases, the flame height is slightly reduced for preheated conditions, which implies a slight increase in kinetic reactivity for the preheated flames. For non-dilute flames, an increase in both the CH* and OH* maximum and integrated intensities are observed for preheated conditions. This increase in emission intensities is thought to be due to the combination of two physical effects. Although CH* and OH* may be born from chemical activation, the increased initial temperature of the reactants raises the electronic partition function of CH and OH molecules in the flame as the electronically excited state becomes more available to these molecules. In this way, a higher population of excited state molecules are contained in the preheated flames causing a larger amount of photons to be released during their quenching back to equilibrium. In addition, the intensities within the spectrally filtered images may be skewed due to the broadband photon emission from excited CO₂ molecules, which tend to become more optically active within specific spectral regions based on varying flame conditions [51]. In general, the addition of DME as a fuel additive has a promoting effect on the reactivity of the doped mixture as compared to the neat fuel [52]. In transient reaction environments where a fresh charge of reactants is oxidized (for example the ignition process), the added DME to the reactants quickly decomposes to produce a large pool of methyl radicals, and thus greatly accelerates the fuel conversion process. A reactivity promoting effect for DME doped conditions has not been observed for the swirl flames investigated in this study, where flame geometries and intensities for the DME doped cases are virtually identical to the neat cases. We hypothesize that the reactivity promoting effects of DME were not observed within the swirl flames presented here as a result of the swirl/turbulence induced at the burner exit, for this particular burner, which efficiently creates a standing, well-mixed radical pool that reactants are added to. This point is an interesting one, and highlights the effectiveness of swirl induction at the burner exit nozzle as a substitute for chemically induced reactivity promotion and flame stabilization.

Generically, changes in both flame geometry and intensity are observed when flames are diluted. The addition of diluents to the air stream causes a systematic reduction in the diameter of the conical reaction zone throughout the vertical axis of the flame. This trend is most likely due to an enhanced swirl-induced confinement of the flame as a result of the added mass flow through the burner. A drastic reduction in the intensity of both maximum and integrated CH* and OH* signals is observed for diluted cases compared to non-dilute cases. This result is most likely caused by a change in two physical conditions of the reacting zone upon the addition of diluents. Firstly, the added thermal mass of diluent gases that do not participate in chemical reactions causes a drop in temperature throughout the reaction zone compared to undiluted cases, which in turn lowers equilibrium access of the electronically excited states to the present CH and OH molecules. Secondly, the added CO₂ and H₂O in the diluent stream act as highly effective collisional partners that can quickly deactivate the excited state species, perhaps upstream of the burner surface that is out of view of the CCD. For diluted cases, no difference is observed in the intensities of flames at varied initial temperatures. It should be noted that the cases displayed in Figs. 10.7, 10.8

and 10.9 consider a dry dilution for the lower initial temperature flames, while a wet dilution was used for the higher temperature flames.

Considering all of the data presented here from a broad point of view, only small changes were detected in both flame geometries and intensities as a function of fuel changes, DME addition, and flame dilution. This seemingly trivial point should not be overlooked under the perspective that these reaction environment variations correlate to, and demonstrate fuel flexibility and mixture dilution stability for swirling, reactive flows. More universally, this finding also highlights the utility of tailored fluid dynamic environments to reduce the sensitivity of fuel chemistry on efficient fuel conversion at kinetically difficult conditions.

10.5 Conclusions

In order to assess the effect of bio-fuel addition and mixture dilution in a variety of fuels, in terms of flame shape and luminosity, a series of experimental swirl flame chemiluminescence measurements were conducted. The fuels investigated included hydrocarbons usually utilized as fuel surrogates for marine and automotive engines, in an attempt to provide information that could be useful for engine studies. More specifically, CH* and OH* chemiluminescence profiles were obtained for all fuels with and without the use of pre-heating, DME addition as a bio derived fuel, diluent addition as an emulated exhaust gas recirculation (EGR) and all these synergistically. These line of sight images were transformed into simplified metrics for flame geometries and intensities, which facilitated a comparison of these properties for the otherwise large experimental matrix. A comparison of these geometrical and chemiluminescent parameters highlighted a chemical uniqueness in methane and propane flames along with a change in flame topology as a function reactant temperature and diluent addition, while the flames were virtually unaffected by all other variations in reaction conditions. This insensitivity provides confidence in the use of tailored in-cylinder fluid dynamic/chemical interactions to extend engine operating conditions to otherwise difficult regimes, while the detailed chemical analysis of more sensitive conditions provides an opportunity for further study.

Acknowledgements

The research leading to these results has received funding from the People Programme (Marie Curie Actions) of the European Unions Seventh Framework Programme FP7/2007-2013/ under REA grant agreement no 607214. All authors are additionally grateful to the SMART-CATS action.

References

- [1] https://unfccc.int/files/essential_background/convention/application/pdf/english_paris_agreement.pdf

- [2] Reitz RD. Directions in internal combustion engine research. *Combust Flame* 2013;1(160):1–8.
- [3] Yao M, Zheng Z, Liu H. Progress and recent trends in homogeneous charge compression ignition (HCCI) engines. *Prog Energy Combust Sci* 2009;35(5):398–437.
- [4] Frusteri F, Spadaro L, Beatrice C, Guido C. Oxygenated additives production for diesel engine emission improvement. *Chem Eng J* 2007;134(1):239–45.
- [5] Saxena S, Bedoya ID. Fundamental phenomena affecting low temperature combustion and HCCI engines, high load limits and strategies for extending these limits. *Prog Energy Combust Sci* 2013;39(5):457–88.
- [6] Tanaka S, Ayala F, Keck JC, Heywood JB. Two-stage ignition in HCCI combustion and HCCI control by fuels and additives. *Combust Flame* 2003;132(1):219–39.
- [7] Flowers D, Aceves S, Martinez-Frias J, Hessel R, Dibble R. Effect of mixing on hydrocarbon and carbon monoxide emissions prediction for isoctane HCCI engine combustion using a multi-zone detailed kinetics solver, SAE Technical Paper; 2003.
- [8] Babajimopoulos A, Assanis D, Flowers D, Aceves S, Hessel R. A fully coupled computational fluid dynamics and multi-zone model with detailed chemical kinetics for the simulation of premixed charge compression ignition engines. *Int J Engine Res* 2005;6(5):497–512.
- [9] Broatch A, Margot X, Gil A, Donayre J. A CFD approach to diesel engine combustion chamber resonance. SAE Technical Paper, Consiglio Nazionale delle Ricerche; 2007. doi:10.4271/2007-24-0043.
- [10] Price P, Stone R, Collier T, Davies M. Particulate matter and hydrocarbon emissions measurements: comparing first and second generation DISI with PFI in single cylinder optical engines. SAE Technical Paper, SAE International; 2006. doi:10.4271/2006-01-1263.
- [11] Zhao H, Ladommatos N. Optical diagnostics for in-cylinder mixture formation measurements in ic engines. *Prog Energy Combust Sci* 1998;24(4):297–336.
- [12] Wimmer A, Pivec R, Sams T, Heat transfer to the combustion chamber and port walls of IC engines - measurement and prediction. SAE Technical Paper, SAE International; 2000. doi:10.4271/2000-01-0568.
- [13] Furuhashi S, Sasaki S. New device for the measurement of piston frictional forces in small engines. SAE Technical Paper, SAE International; 1983. doi:10.4271/831284.
- [14] Singh S, Reitz R, Musculus M, Lachaux T. Validation of engine combustion models against detailed in-cylinder optical diagnostics data for a heavy-duty compression-ignition engine. *Int J Engine Res* 2007;8(1):97–126.
- [15] Aronsson U, Chartier C, Horn U, Andersson Ö et al. Heat release comparison between optical and all-metal HSDI diesel engines. SAE Technical Paper 2008–01-1062; 2008. doi:10.4271/2008-01-1062.
- [16] Founti M, Hardalupas Y, Hong C, Keramiotis C, et al. An Experimental Investigation on the effect of diluent addition on flame characteristics in a single cylinder optical diesel engine, SAE Technical Paper 2015–24-2438; 2015. doi:10.4271/2015-24-2438.
- [17] Fischer S, Dryer F, Curran H. The reaction kinetics of dimethyl ether. i: High- temperature pyrolysis and oxidation in flow reactors. *Int J Chem Kinet* 2000;32(12):713–40.
- [18] Dagaut P, Reuillon M, Cathonnet M. Experimental study of the oxidation of n-heptane in a jet stirred reactor from low to high temperature and pressures up to 40 atm. *Combust Flame* 1995;101(1):132–40.

- [19] Richard S, Dulbecco A, Angelberger C, Truffin K. Invited review: development of a one-dimensional computational fluid dynamics modeling approach to predict cycle-to-cycle variability in spark-ignition engines based on physical understanding acquired from large-eddy simulation. *Int J Engine Res* 2015;16(3):379–402.
- [20] Lehtiniemi H, Mauss F, Balthasar M, Magnusson I. Modeling diesel spray ignition using detailed chemistry with a progress variable approach. *Combust Sci Technol* 2006;178(10–11):1977–97.
- [21] Candel S, Durox D, Schuller T, Palies P, Bourgouin JF, Moeck JP. Progress and challenges in swirling flame dynamics. *C. R. Mecanique* 2012;340:758–68.
- [22] Candel S, Durox D, Schuller T, Bourgouin JF, Moeck J. Dynamics of swirling flames. *Annu Rev Fluid Mech* 46:147–173.
- [23] Lilley DG. Swirl flows in combustion: a review. *AIAA J* 1977;15(8):1063–78.
- [24] Becker LG, et al. Experimental investigation of flame stabilization inside the quarl of an oxyfuel swirl burner. *Fuel* 2016.
- [25] Roy RN, Sreedhara S. A numerical study on the influence of airstream dilution and jet velocity on NO emission characteristics of CH₄ and DME bluff-body flames. *Fuel* 2015;142:73–80.
- [26] Burke MP, Chaos M, Dryer FL, Ju Y. Negative pressure dependence of mass burning rates of H₂/CO/O₂/diluent flames at low flame temperatures. *Combust Flame* 2010;157:618–31.
- [27] Huang Y, Yang V. Dynamics and stability of lean-premixed swirl-stabilized combustion. *Prog Energy Combust Sci* 2009;35(4):293–364.
- [28] Samaniego J-M, Egolfopoulos FN, Bowman CT. CO₂* chemiluminescence in premixed flames. *Combust Sci Technol* 1995;109:183–203.
- [29] Hardalupas Y, Orain M. Local measurements of the time-dependent heat release rate and equivalence ratio using chemiluminescent emission from a flame. *Combust Flame* 2004;139:188–207.
- [30] Docquier N, Belhafaoui S, Lacas F, Darabiha N, Rolon C. Experimental and numerical study of chemiluminescence in methane/air high-pressure flames for active control applications. *Proc Combust Inst* 2000;28:1765–74.
- [31] Higgins B, McQuay MQ, Lacas F, Candel S. An experimental study on the effect of pressure and strain rate on CH chemiluminescence of premixed fuel-lean methane/air flames. *Fuel* 2001;80:1583–91.
- [32] Ayoola BO, Balachandran R, Frank JH, Mastorakos E, Kaminski CF. Spatially resolved heat release rate measurements in turbulent premixed flames. *Combust Flame* 2006;144:1–16.
- [33] Nori VN, Scitzman JM. CH* chemiluminescence modeling for combustion diagnostics. *Proc Combust Inst* 2009;32:895–903.
- [34] Guethe F, Guyot D, Singla G, Noiray N, Schuermans B. Chemiluminescence as diagnostic tool in the development of gas turbines. *Appl Phys B Lasers Opt* 2012;107:619–36.
- [35] García-Armingol T, Hardalupas Y, Taylor AMKP, Ballester J. Effect of local flame properties on chemiluminescence-based stoichiometry measurement. *Exp Therm Fluid Sci* 2014;53:93–103.
- [36] Doss T, Keramiotis C, Vourliotakis G, Zannis G, Skevis G, Founti M. Experimental investigation on the influence of simulated EGR addition on swirl-stabilized CH₄ flames. *J Energy Eng* 2015 E4015008-1-13.
- [37] Orfanoudakis NG, HatziaPOSTOLOU A, Krallis K, Vlachakis N, Design and evaluation measurements of a swirl stabilized laboratory burner. *Proceedings of the Institution of Mechanical Engineers, Part C: Journal of Mechanical Engineering Science* 2005;219(10):1079–1086.

- [38] Nawdiyal A, Hansen N, Zeuch T, Seidel L, Mauss F. Experimental and modelling study of speciation and benzene formation pathways in premixed 1-hexene flames. *Proc Combust Inst* 2015;35(1):325–32.
- [39] Davis S, Law C, Wang H. Propene pyrolysis and oxidation kinetics in a flow reactor and laminar flames. *Combust Flame* 1999;119(4):375–99.
- [40] Roesler J, Martinot S, McEnally C, Pfefferle L, Delfau J-L, Vovelle C. Investigating the role of methane on the growth of aromatic hydrocarbons and soot in fundamental combustion processes. *Combust Flame* 2003;134(3):249–60.
- [41] Basu D, Saha R, Ganguly R, Datta A. Performance improvement of LPG cook stoves through burner and nozzle modifications. *J Energy Inst.* 2008;81(4):218–225.
- [42] Li X, Sun Z, Du W, Wei R. Research and development of double swirl combustion system for a diesel engine. *Combust Sci Technol* 2010;182(8):1029–1049.
- [43] Stoyanov B, Beyazov J. Determination of the flow rate of different fluids by a rotameter. 2005;55.
- [44] Dasch CJ. One-dimensional tomography: a comparison of Abel, onion-peeling, and filtered backprojection methods. *Appl Opt* 1992;31:1146–52.
- [45] Kariuki J, Dawson JR, Mastorakos E. Measurements in turbulent premixed bluff body flames close to blow-off. *Combust Flame* 2012;159:2589–607.
- [46] Sweeney MS, Hochgreb S, Dunn MJ, Barlow RS. The structure of turbulent stratified and premixed methane/air flames II: swirling flows. *Combust Flame* 2012;159:2912–29.
- [47] Souflas K, Paterakis G, Koutmos P. Investigation of disk-stabilized propane flames operated under stratified and vitiated inlet mixture conditions. *J Energy Eng* 2016;142:E4015005.
- [48] Guyot D, Guethe F, Schuermans B, Lacarelle A, Paschereit O. *ASME Turbo Expo 2010*;2(GT2010-23135):933–44.
- [49] Kopp MM, Mathieu O, Petersen EL. *Int J Chem Kinetics* 2014;47:50–72.
- [50] Metcalfe WK, Burke SM, Ahmed SS, Curran HJ. A hierarchical and comparative kinetic modeling study of C₁–C₂ hydrocarbon and oxygenated fuels. *Int J Chem Kinetics* 2013;45:638–75.
- [51] Nori V, Seitzman J. Evaluation of chemiluminescence as a combustion diagnostic under varying operating conditions. In: 46th AIAA Aerospace Sciences Meeting and Exhibit.
- [52] Burke U, Somers KP, O’Toole P, Zinner CM, Marquet N, Bourque G, Petersen EL, Metcalfe WK, Serinyel Z, Curran HJ. An ignition delay and kinetic modeling study of methane, dimethylether, and their mixtures at high pressures. *Combust Flame* 2015;162(2):315–30.